Emissive Organogel Mediated Construction of Flexible Covalent Organic Polymer for the Separation of Aniline for Water Purification

Sayan Maiti, Tapas Ghosh, Arati Samal and Apurba K Das*

Department of Chemistry, Indian Institute of Technology Indore, Khandwa Road, Indore 453552, India

E-mail: apurba.das@iiti.ac.in

Abstract: A flexible covalent organic polymer (**COP**) has been successfully synthesized *via* dynamic covalent gel (DCG) formation through imine condensation reaction between 6-hydrazinonicotinic hydrazide hydrate and benzene-1,3,5-tricarboxaldehyde within 7 min under ambient condition. An emissive organogel mediated protocol has been developed for the construction of amorphous polymer (**COP**), selectively in *N*,*N*-dimethyl acetamide (DMA). Interestingly, two non-emissive building block units without large π-conjugated structures have been engaged for the construction of green emissive **COP-gel**. The green emission of **COP-gel** is generated by the intermolecular H-bonding assisted aggregation induced emission phenomenon. The dried **COP** efficiently adsorbs aniline molecules into its cavities and separate them from binary mixtures of aniline/nitrobenzene and aniline/water, respectively.

Introduction

Covalent organic polymers (COPs) are the unique class of organic porous material that are constructed covalently from organic subunits.[1] Mostly, COPs are constructed from functional organic building blocks through the formation of B-N, B-O, C=N, C=C, C-N, C=N, C=N/C-O, N=N, and Si-O bonds.[2] Several methods or templates such as polymer-to-polymer transformation strategy, transamination reactions of precursors, linker substitution,

interfacial crystallization strategy, cyclization, utilizing a covalent organic gel formation and oxidation have been developed to synthesize COPs.[3] It is still a difficult task to develop alternative synthetic approaches for the synthesis of large-scale COPs under ambient conditions. Aggregation assisted synthetic procedure can be a easiest route for the scalable synthesis of COPs. In general, aggregates can be obtained after the reactions between building block units in three different ways through the formation of (1) crystalline covalent organic frameworks (COFs), (2) amorphous porous organic polymer and (3) gels. Gels are formed through the intermediate aggregates between crystalline COFs and amorphous COPs. However, it is a challenging task to evaluate the nature of covalent dynamic gels, despite their various applications in catalysis, sensors and adsorbent materials.[4]

The properties of COPs can be modified at the atomic level by using the appropriate monomers. In order to extend the implementation of porous organic polymers, time-efficient synthetic method is being sought. Covalent organic polymers (COPs)[5] have received considerable importance due to their potential use in many areas.[6] In this regard, the introduction of various functional groups into porous materials have been reported as an effective way to improve their adsorption capacity and selectivity towards organic molecules. The efficient separation of aromatic organic solvent from solvent mixtures and their derivatives, which are critical components of the chemical industry, can lead to higher reusability. Aniline is a crucial intermediate in the manufacture of pharmaceuticals products, rubber accelerators, and anti-aging compounds.[7] Moreover, aniline is a common organic contaminant with high toxicity, rapid bio-enrichment, and challenging biodegradability.[8] Since aniline possesses potential danger in industrial scale separation, human health and environment due to their high toxicity, volatility or flammability, there is a strong demand for the development of new highly effective and environmentally safe materials for the separation of aniline from solvents mixture.[9] A wide range of methods and technologies

have been developed to remove aniline.[10] On the other hand, several nitrogen atom containing recyclable green switchable solvents are widely used for the extraction or separation of organic solvents.[11] However, most of the switchable solvents are amines that separate the desire product from the solvent mixtures through a phase transition process. Li et al used nitrogen containing ionic liquids for the separation of binary mixture by extractive distillation methods.[12] The extractive distillation method is also allowed to separate organic solvent mixtures.[13] Although above mentioned methods or processes are quite complicated and characterized by high energy consumption and high equipment cost.[13b] Therefore, it is necessary to develop a convenient method and material with lower equipment costs for the separation of organic solvents. In this regard, adsorption using solid adsorbent is a quick and easy method,[10] and nitrogen functionalized COP can be the innovative solid adsorbent material with high adsorption capacity and selectivity for the separation of organic solvents. The adsorption technique is demonstrated to be enhanced with a better adsorption capacity and selectivity due to the possible H-bonding, electrostatic and acid-base interaction between the surface functional groups on the COPs and adsorbates. Herein, our objectives are (1) to develop new synthetic methodologies with large-scale synthesis of functionalized COP materials under ambient condition, (2) to develop cavities inside the COP backbone through dynamic covalent gel (DCG) strategy and (3) to execute the intrinsic properties of functionalized COP materials. In this work, we have synthesized hydrazine, hydrazide and pyridine groups functionalized **COP** *via* emissive organogel formation within 7 min (Figure 1a). We have investigated the photophysical characteristics of emissive **COP-gel** and **COP** in DMA solution in presence of nitrobenzene and aniline. The gel formation plays a key role for synthesizing the **COP** in large scale. The **COP** is capable to adsorb or encapsulate aniline selectively in its cavities and selectively separate from binary mixtures of aniline/nitrobenzene and aniline/water.

Results and Discussion

Here we have developed a facile synthetic strategy to synthesize covalent organic polymer with the 6-hydrazinonicotinic hydrazide hydrate and benzene-1,3,5-tricarboxaldehyde as building block units. The **COP** has been synthesized *via* emissive organogel formation in DMA under acidic condition within 7 min (Figure 1a) under ambient condition. The gel is formed with the **COP** concentration of about 0.038-0.040 mol L^{-1}. Among ethyl acetate (EtOAc), diethyl ether (Et_2O), ethylene glycol $(CH_2OH)_2$, methanol (MeOH), N,N-dimethyl acetamide (DMA), dichloromethane (CH_2Cl_2) and dimethyl sulfoxide (DMSO), the **COP** was successfully formed in DMA *via* emissive gel formation (Figure 1). Figure S1 shows 3D block representation of **COP-gel**. To obtain pure **COP**, the **COP-gel** was dried and washed several times with water, ethyl acetate, N,N-dimethyl formamide, and methanol. After drying at 90 °C, the **COP** was characterized using several techniques.

The FT-IR spectrum of **COP** demonstrates the successful construction of **COP** *via* the formation of -C=N bond.[14] The peaks at 1530, 1605 cm^{-1} are assigned to -C=C- and -C=N bonds stretching. A peak at 1650 cm^{-1} is appeared due to -C(=O)NHNH- stretching band (Figure 2a). The powder XRD pattern of **COP** suggests that the polymer is successfully constructed from two crystalline secondary building block units (Figure S2a). The broad powder XRD pattern of **COP** assigns its amorphous polymeric nature (Figure 2b). A slight broad peak at higher 2θ indicates to the strong π-π stacking interaction between the **COP** layers. To account the thermal stability of **COP**, we have performed thermogravimetric analysis (Figure 2c). The **COP** exhibits high thermal stability. The TGA spectrum of **COP** shows a 4% weight loss at lower temperature range from 27 to 200 °C due to the evaporation of residual solvents, followed by the weight loss of 6.34% and 15.95% over the temperature range of 200 to 370 °C and 370 to 402 °C respectively. Following that, a gradual loss of weight is observed as the temperature goes up.

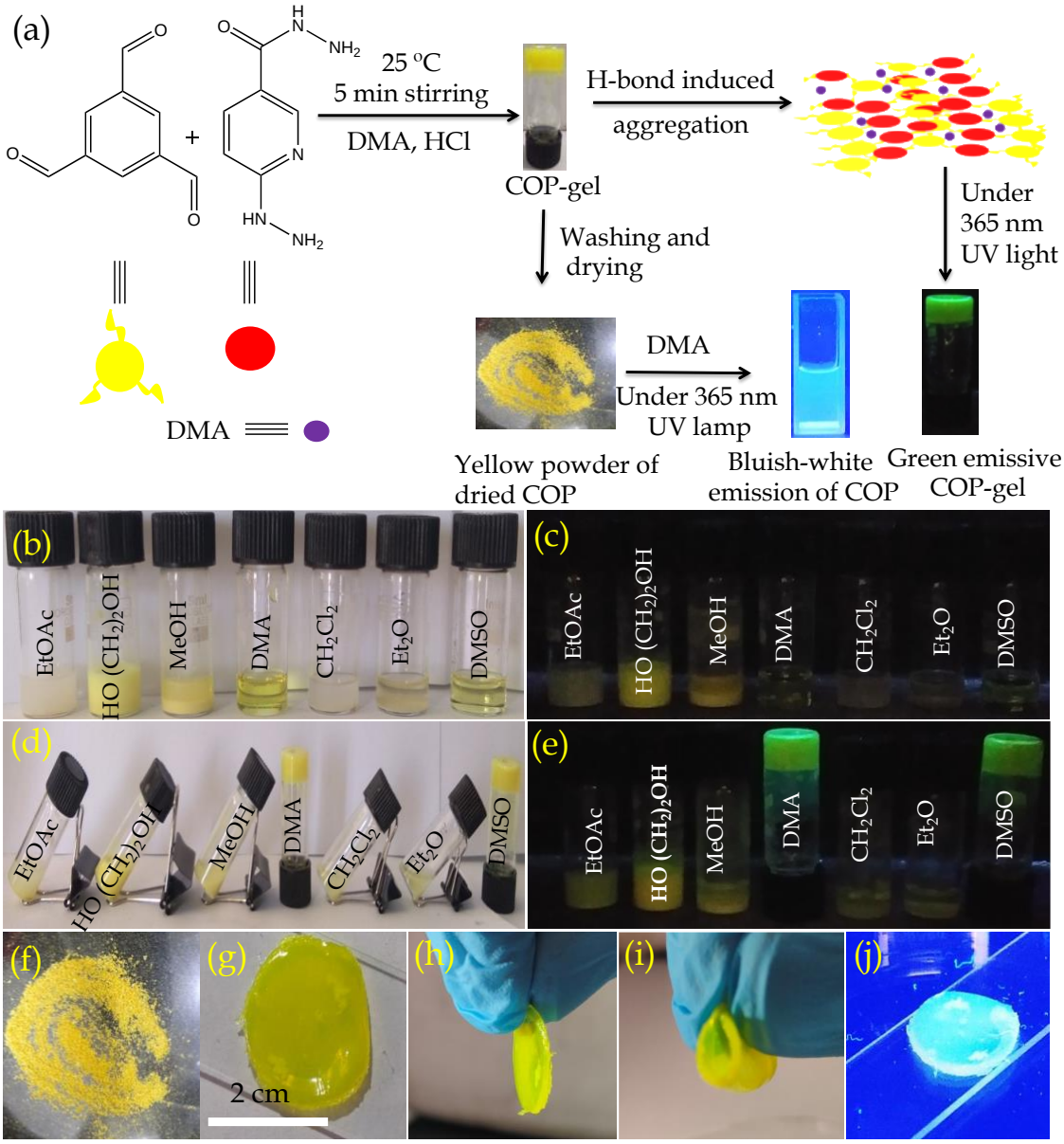

Figure 1. (a) Schematic representation of porous **COP** synthesis, and aniline separation and adsorption by **COP**. Solution mixture of 6-hydrazinonicotinic hydrazide hydrate and benzene-1,3,5-tricarboxaldehyde in different solvents (b) in day light and (c) under 365 nm UV light. Solution mixture of 6-hydrazinonicotinic hydrazide hydrate and benzene-1,3,5-tricarboxaldehyde in different solvents after the addition of 1N HCl (d) in day light and (e) under 365 nm UV light. Optical images of (f) **COP** powder, (g-j) films formed with **COP** and (i) **COP** film (shows white-cyan colour emission) under 365 nm UV light.

The solid-state 13C CP-MAS NMR of **COP** also supports the successful formation of **COP** (Figure 2d). The peaks from 120-140 ppm confirm the presence of phenyl groups. The peak at 159 ppm suggests acylhydrazone groups in **COP**. The peak at 163 ppm confirms the presence of carbonyl group of -C(O)NHNH- and a peak at 150 ppm is appeared due to C=N bond of pyridine ring.[44] The porosity of **COP** was evaluated by performing BET surface area analysis by N_2 sorption at 77 K and 1 bar pressure. No hysteresis loop is observed in the isotherm. The **COP** shows type II reversible isotherm (Figure S2b). The presence of micropores is demonstrated by a steep uptake at a low relative pressure P/P_0. This result clearly suggests that microporosity has been grown inside the **COP** during the gel formation. At high relative pressures of $P/P_0 > 0.9$, a significant volume of N_2 adsorption is observed. The increase in N_2 adsorption at $P/P_0 > 0.9$ and the complete absence of saturation in the adsorption isotherm can be ascribed to the condensation of N_2 gas molecules in inter-particular voids or in larger pores. The calculated surface area of **COP** is 645.9 $m^2 g^{-1}$ (Table S1). The pore size distribution of **COP** was studied *via* NLDFT method (Figure S3). The calculated pore volume of **COP** is 0.49 $cc.g^{-1}$. The rheology of **COP-gel** was performed at ambient temperature to evaluate the mechanical properties of **COP-gel** (Figure 2e and 2f). The oscillatory frequency was performed at frequency range of 0.05 to 100 rad s^{-1} at an applied strain of 1%. The storage modulus (G') is significantly higher than the loss modulus (G'') over the studied frequency range which clearly indicates the viscoelastic and robustness nature of **COP-gel**.

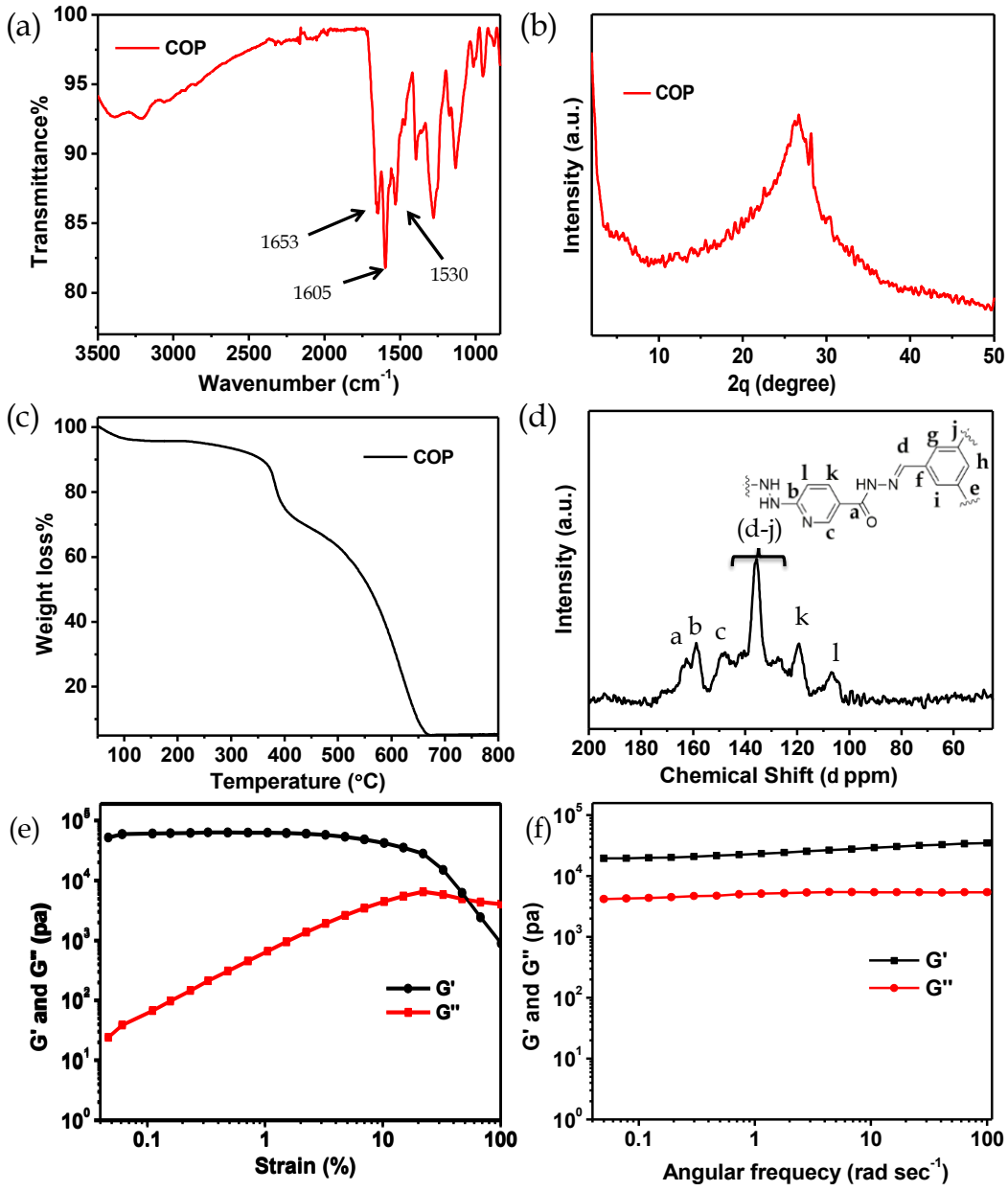

Figure 2. (a) FT-IR spectrum of **COP**. (b) Powder XRD pattern of **COP**. (c) TGA of **COP**. (d) Solid state 13C NMR spectrum of **COP**. Linear viscoelastic (LVE) properties of (e) **COP-gel** and (f) the dynamic frequency sweep experiment of **COP-gel.**

According to scanning (SEM) and high resolution transmission electron microscopy (HRTEM), **COP** generates a sponge-like porous structure made up of interconnected nanoscale spherical particles (Figure 3a and 3b). The particles with a diameter of 20-40 nm combine to form a three-dimensional gel matrix. The surface hydrophobicity and surface

roughness of **COP** was evaluated using atomic force microscopy (Figure 3c). The nano level surface roughness illustrates the hydrophobicity of **COP**. In general, highly hydrophobic materials have tendency to aggregate into spherical assembly upon coating on glass surface.[15] Similarly, the **COP** also shows this salient features. The **COP** surface contains several crests and troughs which have been observed from the 3D view (Figure 3d). The peaks in the region of 0.5 μm indicate the existence of air pockets between the peaks (valley regions). These trapped air pocket in the valley region creates the hydrophobic pore in **COP**.

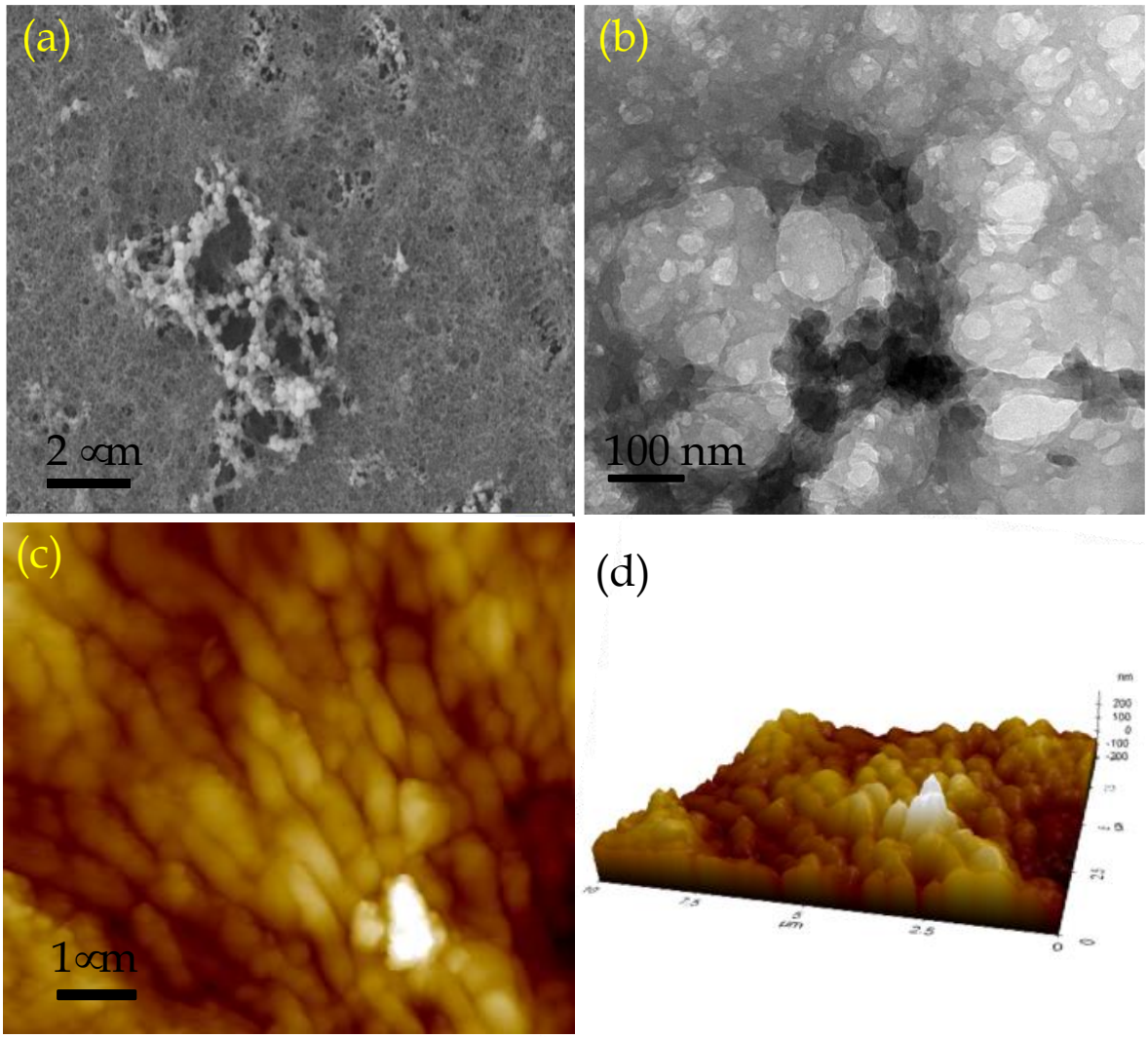

Figure 3. a) SEM, (b) HRTEM images of COP. (c) AFM image of COP and (d) 3D AFM (Z-axis interpretation) image of COP.

The **COP-gel** shows green emission within the range of 520-550 nm. Interestingly two secondary building block units are non-fluorescent in DMA solvent and the pyridine moiety is itself a fluorescence quencher. The **COP** backbone is rigidified through a series of H-bonding interaction between the hydrazide groups and the solvent molecule (DMA) (Figure S4). These H-bonds are highly responsible for the restriction of intramolecular rotation, which causes aggregation-induced emission (AIE).[16] The emission color of **COP** originates from distinct level of aggregation in solvent which alters the electronic distribution and shows different fluorescent color. So, H-bonding plays a significant role in the evolution of emissive **COP-gel**. By varying the concentration of building block units, we have also prepared **COP** through flexible thin film preparation in DMA solvent. Different extent of aggregation is occurred in gel and thin film that leads different emission colors (Figure 1g and 1i). We have investigated detailed spectroscopic study to prove the H-bonding induced strong aggregation in **COP-gel**. The UV-vis spectrum of **COP-gel** shows an absorption maximum centered at 311 nm, which is attributed to the n-π^* transition (Figure S5). On the other hand, an absorption peak at 423 nm of **COP-gel** is observed, which suggests the formation of strong intermolecular H-bonds. This phenomenon indicates its higher order aggregated state by restricting intramolecular rotation (RIR) and lowering the HOMO-LUMO energy gap.[17] Also, a broader absorption band reveals higher order aggregated form of **COP-gel** (Figure S5). The **COP-gel** shows dual emission at 530 nm with a shoulder peak at 626 nm (Figure S6). We have also performed temperature dependent fluorescence studies of **COP-gel**. The temperature-dependent fluorescence studies reveal that emission intensity decreases gradually with the increase in temperature (Figure S7). These results also support the existence of H-bonding inside the **COP-gel**. The excitation spectrum of **COP-gel** at 530 nm is similar with the excitation spectrum of **COP-gel** at 626 nm (Figure S8). These results indicate that the origin of shoulder band at around 626 nm of **COP-gel** is assigned to the

protonated state.[18] An emission peak at 626 nm originates from the protonated form of the **COP-gel** (due to formation of the PyH^+ and imine -C=NH^+-). The green color emission of **COP-gel** is also visualized under confocal microscope with the excitation wavelength of 405 nm and emission collection of 540 nm respectively. The confocal image of **COP** is shown in Figure S9. Confocal images further support the AIE phenomenon in solid state of **COP** in green color region.[19] We have further investigated the photophysical properties of disperse solutions of **COP** powder in DMA solution. As previously stated, the introduction of hydrazide functionality is crucial for strengthening the **COP's** emissive behaviour *via* strong intra- and interlayer H-bonding interactions. In the UV-vis spectra of **COP** solution, a broad absorption maximum is found across the wavelength range of 300 to 400 nm, which correlates to the n-π^* transitions and also reveals its aggregated state (Figure S10). For an excitation wavelength of 340 nm, the emission spectra of **COP** in DMA shows a maximum at 474 nm (Figure S10). Pyridine and hydrazide functionalized **COP** showcased adequate thermal and chemical stability due to the presence of several heteroatoms in the polymeric backbone, and H-bonding controlled fluorescence property in DMA solution. The abundant heteroatoms form intra- and intermolecular H-bonds, causing aggregation, limiting intermolecular rotation, and emitting light. The emission intensity of **COP** is higher in DMA solution, which is clearly attributed to intermolecular or intermolecular H-bonding assisted aggregation induced emission properties.

Solvent extraction method is widely used to isolate aromatic organic solvent mixtures and their derivatives. The choice of material is highly influenced by its similarity to the target product, cost and safety. Nitrogen-rich switchable materials, a type of recyclable green materials, can be used to separate the organic solvent mixtures in efficient cost-effective manner.[21] Herein, the **COP** acts as an efficient stationary phase for the separation of organic solvents from binary organic solvent mixtures (Figure 4 and Figure S11). We have taken

aniline/nitrobenzene as model organic solvent mixture for the separation experiment using dried **COP**. Initially, we loaded 60 mg of **COP** inside 1 mL (5.5 cm) glass syringe and packing length was 0.15 mL (0.7 cm). At first, we took 50 μL of each solvent and diluted it with hexane and passed through the **COP** loaded in 1 mL glass syringe. The **COP** selectively adsorb and separate aniline from nitrobenzene. Hexane was used as mobile phase solvent. All the filtrates were characterized by high performance liquid chromatography (HPLC) (Figure S12-S13). Generally, separation of the organic solvents depend on the surface charge of the **COP**, pore size, functionality on the **COP** surface and electrostatic interactions between **COP** and organic solvents. Here, the **COP** exhibits hydrazide and pyridinic groups rich surface with average pore size distribution of 1.3 to 10 nm.[22]

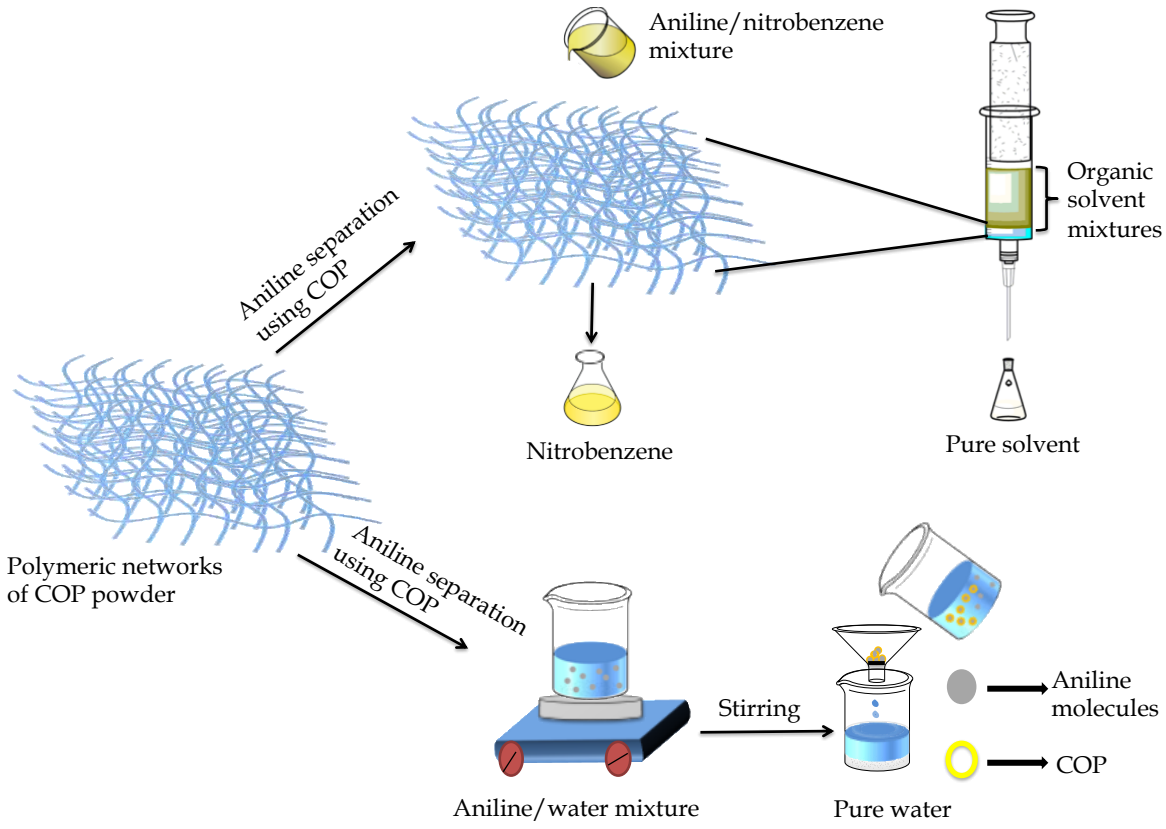

Figure 4. Schematic representation of aniline separation from binary solvent mixtures aniline/nitrobenzene and aniline/water.

Aniline shows high binding interactions and easily stack with the **COP** backbone through -NH···N- interactions that also induces the aggregation properties of **COP** and reside in the pore cavity of the polymer.[23] Nitrobenzene, on the other hand, lacks any polar amine ($-NH_2$) group and is unable to bind with the **COP** backbone. As a result, nitrobenzene can easily escape *via* the **COP**. Hexane (6 mL) is required to remove the entire amount of nitrobenzene. We have also investigated the adsorption limit of aniline over 60 mg **COP** powder. The high adsorption limit of **COP** is found as 55 μL/60 mg for aniline. After each cycles, loaded **COP** powder (stationary phase) was washed very well with the water, ethyl acetate and methanol to remove adsorbed solvent (aniline) from the pore of **COP**. After that used **COP** was dried under 90 ºC and used for next cycle. The **COP** was reused and the **COP** retains its activity after five cycles (Figure S14). For the purpose of the extraction of aniline from aniline/water mixture, we have directly used the resultant **COP** powder. The adsorption mechanism was followed to extract aniline where **COP** acts as adsorbent for the aniline in aqueous solution. Here, 45 mg of **COP** powder was added to a 3 mL aqueous solution of aniline with the concentration of 222 mg L^{-1} and allowed to stir at 25 ^{0}C. UV-Vis spectra of the resultant solution were recorded at different time intervals. The gradual decrease in aniline absorbance suggests quick adsorption performance (Figure. S15a). The **COP** exhibits significant adsorption performance for aniline, removing 83.5% of aniline in 8 h and achieves adsorption equilibrium (using Eq. S1). The removal rate of **COP** for aniline is substantially higher, implying that $-NH_2$ group of aniline plays a crucial role in the adsorption process towards **COP** functionalities. Compared with the nitrobenzene, the **COP** is the better adsorbent material with fast adsorption for aniline, which is due to the well-defined porous structure and surface functionalities. The adsorption process demonstrates that the incorporated hydrazide groups of **COP** are favourable for adsorption due to possible H-bonding and acid-base interactions.

Conclusion

In summary, we synthesized covalent organic polymer (**COP**) via dynamic covalent gel (DCG) through imine bond formation. *N*,*N*-dimethyl acetamide showed a significant role for the scalable synthesis of **COP** *via* gel formation. The emissive gel served as an interesting protocol for the construction of porous **COP**. The green emission of **COP-gel** was caused by an aggregation-induced emission (AIE) phenomenon, which was assisted by H-bonding and several non-covalent interactions. On the other hand, the disperse solution of **COP** in DMA showed bluish-white light emission. The degree of aggregation was important in determining the emission color of **COP** in gel and solution states. The dried **COP** had the ability to easily adsorb aniline molecules into its cavities and separate them from binary mixtures of aniline/nitrobenzene and aniline/water. Our findings represent a significant advancement in the development of functionalized **COP** with excellent scalability under ambient conditions, as well as significant physical insights for the separation of aniline from miscible binary solvent mixtures.

Acknowledgement

The authors gratefully acknowledges CSIR, Government of India (Project No. 01(2936)/18/EMR-II) for financial support and SIC, IIT Indore for providing the required instrumental facilities. SM thanks IIT Indore, TG acknowledges DST Inspire Fellowship, Government of India and AS acknowledges CSIR, Government of India for their doctoral fellowship.

References

[1] P. Puthiaraj, Y.-R. Lee, S. Zhang, W.-S. Ahn, *J. Mater. Chem. A*, **2016**, *4*, 16288-16311.

[2] a) V. S. Vyas, F. Haase, L. Stegbauer, G. Savasci, F. Podjaski, C. Ochsenfeld,B. V. Lotsch, *Nat. Commun*. **2015**, *6*, 8508. b) P. Wang, F. Zhou, C. Zhang, S.-Y. Yin, L. Teng, L. Chen, X.-X. Hu, H. W.Liu, X. Yin, X.-B. Zhang, *Chem. Sci*. **2018**, *9*, 8402–8408.

[3] a) Z. Miao, G. Liu, Y. Cui, Z. Liu, J. Li, F. Han, Y. Liu, X, Sun, X. Gong, Y. Zhai, Y. Zhao, Y. Zeng, *Angew. Chem., Int. Ed*. **2019,** *58*, 4906-4910. b) C. Qian, Q.-Y. Qi, G.-F. Jiang, F.-Z. Cui, Y. Tian, X. Zhao, *J. Am. Chem. Soc*. **2017**, *139*, 6736-6743. c) W. Luo, Y. Zhu, J. Zhang, J. He, Z. Chi, P. W. Miller, L. Chena, C.-Y. Su, *Chem. Commun*. **2014**, *50*, 11942- 11945.

[4] a) H. Fang, L. Chen, L. Zeng, Z. Yang, J. Zhang, *Global Challenges* **2019**, *3*, 1800073.b) H. Zhong, Y. Gong, W. Liu, B. Zhang, S. Hu, R. Wang, *Dalton Trans*. **2019**, *48*, 2345-2351.

[5] a) S. Das, P. Heasman, T. Ben, S. Qiu, *Chem. Rev*. **2017**, *117*, 1515–1563. b) L. Tan, B. Tan, *Chem. Soc. Rev*. **2017**, *46*, 3322–3356.

[6] a) W. Wang, M. Zhou, D. Yuan, *J. Mater. Chem*. A **2017**, *5*, 1334-1347. b) Q. Chen, M. Luo, P. Hammershøj, D. Zhou, Y. Han, B. W. Laursen, C. Yan, B. Han, *J. Am. Chem. Soc*. **2012**, *134*, 6084–6087. c) Y. Yuan, F. Sun, L. Li, P. Cui, G. Zhu, *Nat. Commun*. **2014**, *5*, 4260. d) X. Li, L. Jin, L. Huang, X. Ge, H. Deng, Y. Li, L. Chai, S. Ma, *J. Envi. Chem. Eng*. **2021**, *9*, 106357. e) P. Samanta, A. V. Desai, S. Let, S. K. Ghosh, *ACS Sustainable Chem. Eng*. **2019**, *7*, 7456-7478. f) K. Dey, S. Kunjattu H, A. M. Chahande, R. Banerjee, *Angew. Chem. Int. Ed*. **2020**, *59*, 1161-1165. g) D. Dey, P. Banerjee, *New J. Chem*. **2019**, *43*, 3769-3777.

[7] D.-W. Gao, Q. Hu, H. Pan, J. Jiang, P. Wang, *Biores. Technol*. **2015**, *193*, 507-512.

[8] F. An, X. Feng, B. Gao, *J. Hazard. Mater*. **2010**, *178*, 499-504.

[9] a) K. Yang, W. Wu, Q. Jing, L. Zhu, Environ. *Sci. Technol*. **2008**, *42*, 7931-7936. b) Y. Zhou, X. Gu, R. Zhang, J. Lu, *Ind. Eng. Chem. Res*. **2014**, *53*, 887-894.

[10] a) Y. Chen, B. Wang, X. Wang, L.-H. Xie, J. Li, Y. Xie, J.-R. Li, *ACS Appl. Mater. Interface* **2017**, **9**, 27027-27035. b) S. H. Gheewala, A. P. Annachhatre, *Water Sci. Technol.* **1997**, *36*, 53-58.

[11] a) P. G. Jessop, S. M. Mercer, D. J. Heldebrant, *Energy Environ. Sci*. **2012**, *5*, 7240-7253. b) G. J. Philip, L. Phan, A. Carrier, S. Robinson, J. D. Christoph, R. H. Jitendra, *Green Chem*. **2010**, *12*, 809-814. c) P. G. Jessop, C. A. Eckert, C. L. Liotta, D. J. Heldebrant, *US Pat*. 2008/005849A1, United States Patent Application Publication, 2008.

[12] W. Li, B. Xu, Z. Lei, C. Dai, *Chem. Eng. Process*. **2018**, *126*, 81-89.

[13] a) W. Ma, J. Sun, W. Hongpu, R. Wang, *Appl. Chem. Ind*. **2010**, *39*, 781-782. b) J. Gu, X. You, C. Tao, J. Li, W. Shen, J. Li, *Chem. Eng. Res. Des*. **2018**, *133*, 303-313.

[14] a) F. J. U.-Romo, C. J. Doonan, H. Furukawa, K. Oisaki, O. M. Yaghi, *J. Am. Chem. Soc*. **2011**, *133*, 11478-11481. b) S. Maiti, A. Roy Chowdhury, A. K. Das, *ChemNanoMat.* **2019**, *6*, 99-106. c) S. Maiti, B. Mandal, M. Sharma, S. Mukherjee, A. K. Das, *Chem. Commun*. **2020**, *56*, 9348-9351.

[15] A. Roy Chowdhury, S. Maiti, A. Mondal, A. K. Das, *J. Phys. Chem. C* **2020**, *124*, 7835-7843.

[16] a) S. Dalapati, E. Jin, M. Addicoat, T. Heine, D. Jiang, *J. Am. Chem. Soc*. **2016**, *138*, 18, 5797-5800. b) D. Wang, S.-M. Li, Y.-F. Li, X.-J. Zheng, L.-P. Jin, *Dalton Trans*. **2016**, *45*, 8316-8319.

[17] a) S. Riebe, C. Vallet, F. v. Vight, D. G.-Abradelo, C. Wölper, P.-D. C. A. Strassert, G. Jansen, S. Knauer, J. Voskuhl, *Chem. Eur. J*. **2017**, *23*, 13660-13668. b) H.-Q. Yin, F. Yin, X.-B. Yin, *Chem. Sci*. **2019**, *10*, 11103-11109.

[18] F.-Z. Cui, J.-J. Xie, S.-Y. Jiang, S.-X. Gan, D.-L. Ma, R.-R. Liang, G.-F. Jiang, X. Zhao, *Chem. Commun*. **2019**, *55*, 4550-4553.

[19] S. Feng, S. Gong, G. Feng, *Chem. Commun*. **2020**, *56*, 2511-2513.

[20] L. Deng, X. Kang, T. Quan, L. Yang, S. Liu, K. Zhang, M. Gao, Z. Xia, D. Gao, *ACS Appl. Mater. Interfaces* **2021**, *13*, 33449-33463.

[21] Y. Liu, Z. Qiu, H. Zhong, X. Zhao, W. Huang, X. Xing, *RSC Adv*. **2020**, *10*, 12953-12961.

[22] a) S. Ravi, P. Puthiaraj, K. Yu, W.-S. Ahn, *ACS Appl. Mater. Interfaces* **2019**, *11*, 11488-11497. b) P. Song, Z. Zhang, L. Yu, P. Wang, Q. Wang, Y. Chen, *New J. Chem.* **2020**, *44*, 8572-8577.

[23] a) J.-X. Zhou, X.-S. Luo, X. Liu, Y. Qiao, P. Wang, D. Mecerreyes, N. Bogliotti, S.-L. Chen, M.-H. Huang, *J. Mater. Chem. A* **2018**, 6, 5608-5612. b) Y. Liu, X. Fan, X. Jia, B. Zhang, H. Zhang, A. Zhang, Q. Zhang, *J. Mater. Sci*. **2016**, *51*, 8579-8592. c) A. R. A. Hamid, R. Mhanna, R. Lefort, A. Ghoufi, C. Alba-Simionesco, B. Frick, D. Morineau, *J. Phys. Chem. C* **2016**, *120*, 9245-9252. d) C. A. Hunter, *J. Mol. Biol*. **1993**, *230*, 1025-1054.